

# Spin imaging of Poiseuille flow of viscous electronic fluid

K.S. Denisov,\* K.A. Baryshnikov, and P.S. Alekseev  
*Ioffe Institute, 194021 St.Petersburg, Russia*

(Dated: May 6, 2022)

Recent progress in fabricating high-quality conductors with small densities of defects has initiated the studies of the viscous electron fluid and has motivated the search for the evidences of the hydrodynamic regime of electron transport. In this work we come up with the spin imaging technique allowing us to attest to the emergence of electron hydrodynamic flows. Based on numerical calculations we demonstrate that the injected electron spin density is inhomogeneous across the channel when the viscous electron fluid forms the Poiseuille flow. We also argue that the Hanle curves at different positions across the channel acquire relative phase shifts resulting from the variation of the electron drift velocity in inhomogeneous hydrodynamic flows. The studied effects can be employed to evidence and study the viscous electron fluid non-invasively.

In high-quality conductors with small densities of defects, electrons can form a viscous fluid at low temperatures due to frequent electron-electron collisions and/or elasticity effects from the inter-particle interaction. The charge transport in such fluid is carried out by inhomogeneous hydrodynamic flows, controlled by particular shapes of samples, while its resistance becomes proportional to the viscosity coefficient. These ideas were first proposed and partially theoretically studied for bulk metals with strong electron-phonon coupling [1]. Recently, this topic has become of interest as the hydrodynamic regime of electron transport has been realized in high-quality samples of graphene [2–8], quasi-two dimensional metal PdCoO<sub>2</sub> [9], Weyl semimetal WP<sub>2</sub> [10], and high-mobility GaAs quantum wells [11–23]. These experiments motivated many theoretical works (see, for example [24–40]), which were aimed to formulation and search for the evidences of the hydrodynamic regime as well as to studying of various types and regimes of flows of the electron fluid.

The evidences of formation of a viscous electron fluid are based, first, on an inhomogeneity of space distributions of its flows, leading to the specific properties of observed sample resistances. The simplest of these properties is the cubic dependence of the conductance on the sample width. This dependence was observed for the first time in [9] for stripes of PdCoO<sub>2</sub>. In samples of peculiar geometry of edges and contacts, whirlpools can appear, similarly to water flows in rivers. Herewith opposite direction of the current and the voltage drop appear for some pairs of contacts. This effect of the “absolute negative resistance” was proposed as an evidence of viscous flows of electrons in [6] and was observed for graphene samples in [2]. Second, the dependencies of the electron viscosity on magnetic field and flow frequency are very specific and can be used to characterize the viscous electron fluid. The giant negative magnetoresistance observed on high-mobility GaAs quantum wells [11–14] was explained by this effect and thereby was employed to detect the hydrodynamic transport [15]. For ac flows of the

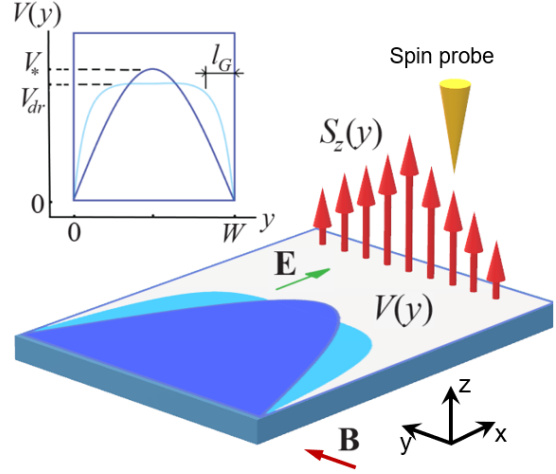


FIG. 1. Scheme of the proposed spin imaging technique. Blue and bright blue curves depict the electron flow velocity  $V(y)$  under electric field  $\mathbf{E}$  for Poiseuille and Ohmic regimes, respectively. The spin polarization  $S_z(y)$  (indicated by red arrows) keeps an inhomogeneous structure at some distance from the injector due to hydrodynamic flow of electrons and can be detected by a local spin probe. Applying an in-plane magnetic field  $\mathbf{B}$  one additionally detects the phase shifts in the Hanle curves tracked at different positions across the sample due to the variation of  $V(y)$ , here  $V_* = V_x(W/2)$ .

electron fluid, the viscosity exhibits the resonance at the doubled electron cyclotron frequency [37, 38]. Such resonance manifests itself in responses of its conductance on incident radiation, that was apparently observed in [21–23]. In particular in a strongly non-ideal electron fluid the ac flow is formed by transverse shear stress waves, whose dispersion law reflects the resonance in the viscosity coefficients. In recent works [7, 8] direct observations of the profiles of the Hall electric field and the current density for a Poiseuille flow of 2D electrons in graphene stripes by means of space resolved measurements of electric and magnetic field were reported.

All these methods are quite difficult to use: they require either an analysis of data on a number of specially designed samples with a given geometry or apply-

\* denisokonstantin@gmail.com

ing sufficiently strong magnetic fields. Therefore, simpler, weaker-invasive methods are wanted.

In this work we propose a spin-injection-based method to detect the hydrodynamic regime of electric transport in an electron fluid (see Fig. 1). We argue that the space distribution of the injected spins in a pure sample can be employed to visualize a viscous flow ("spin imaging technique"). Namely, the distributions of the electron spin density and its magnetic field dependence for the Poiseuille flow of the viscous electron fluid, being inhomogeneous by the section of a sample, strongly differs from the Ohmic regime. We demonstrate this concept by performing the numerical calculations with realistic parameters for high-mobility samples. The advantage of the proposed method is that the injected spin distribution provides almost no effect on the magnitude and profile of a given electron flow. In this way, the proposed technique is "light and non-invasive", as compared with the already existing methods of detection of the viscous electron fluid.

We consider a flow of 2D viscous electron fluid in high-mobility samples, where the time of electron scattering on impurities can be longer than that corresponding to electron-electron collisions. In this regime the electron momentum relaxation takes place predominantly or mostly at the channel boundaries with the subsequent formation of the Poiseuille flow. In case of long and sufficiently wide samples (realized, for example, in experiments [7, 8, 16–18]) the velocity distribution can be found from the Navier-Stokes equation. The result for low-frequency flows in samples with some density of disorder and fully rough edges takes the form [1]:

$$V_x(y) = \frac{e E_x}{m \tau_{tr}} \left\{ 1 - \frac{\cosh[(y - W/2)/l_G]}{\cosh[(W/2)/l_G]} \right\}, \quad (1)$$

where  $m$  is an electron effective mass,  $W$  is the channel width,  $\tau_{tr}$  is the momentum relaxation time in the bulk due to scattering of electrons on disorder or phonons,  $l_G = \sqrt{\eta \tau_{tr}}$  is the Gurzhi length,  $\eta = v_F^2 \tau_{ee}/4$  is the viscosity of the electron fluid determined by the electron-electron collisions time,  $\tau_{ee}$  is the time of relaxation of the shear stress due to inter-particle collisions, and  $v_F$  is the Fermi velocity. Equation (1) describes the homogeneous Ohmic flow  $V_{Ohm} = e E_x / (m \tau_{tr})$  at  $l_G \ll W$ , while the Poiseuille parabolic distribution appears in the opposite limit  $l_G \gtrsim W$  (see Fig. 1).

In this work we address to systems with no pronounced effects of spin-orbital coupling on electric current distribution and neglect the extra-boundary spin accumulation due to the spin Hall effect [41, 42] or any rotational viscosity effects [43–47]. The latter could lead to a vorticity of the electron flow, which induces a torque acting on electron spin and results in generation of the spin density [48]. By other words, our consideration is valid for systems where the electric current profile is settled according to Eq. (1), while the distribution of the spin density follows the local drift velocity of the electron fluid and does not affect its orbital motion. In this approxima-

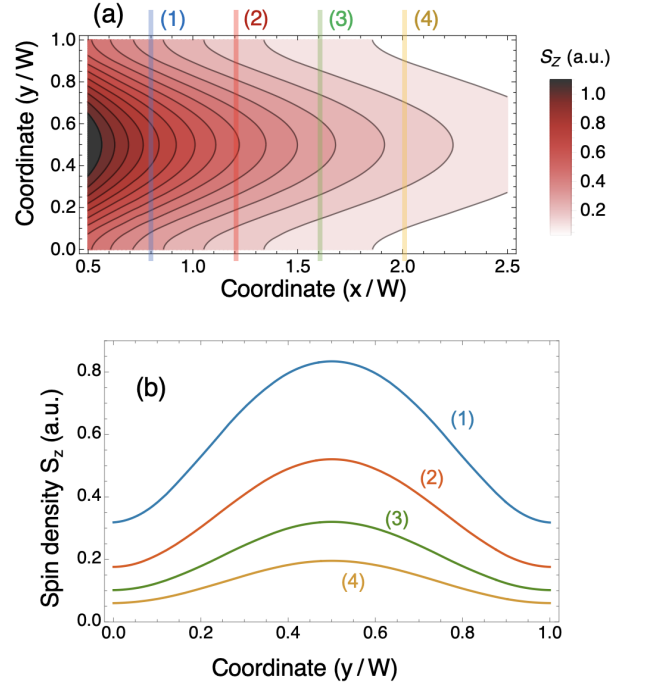


FIG. 2. (a): Calculated distribution of viscous electron fluid spin polarization in the channel. (b): Profiles of the spin density at different  $x$ -positions:  $x = 0.8W$  (1),  $x = 1.2W$  (2),  $x = 1.6W$  (3), and  $x = 2W$  (4). The parameters  $\tau_s = 200$  ps,  $D_s = 60$  cm<sup>2</sup>/s ( $L_s \approx 1.1$   $\mu$ m),  $V_* = 4 \times 10^6$  cm/s ( $L_d = 8$   $\mu$ m) and  $W = 8$   $\mu$ m.

tion the distribution of the spin density  $\mathbf{S}$  can be determined based on the drift-diffusion model [49] formulated in the following equation

$$\dot{\mathbf{S}} + \nabla_i \mathbf{q}^i = [\boldsymbol{\omega}_c \times \mathbf{S}] - \mathbf{S}/\tau_s \quad (2)$$

where  $\mathbf{q}^i$  is the spin current (the flow of the value  $\mathbf{S}$  along the direction  $x_i$ ),  $\boldsymbol{\omega}_c$  is the Larmor precession frequency due to the in-plane magnetic field, and  $\tau_s$  is the spin relaxation time, which is assumed to be isotropic. The spin current  $\mathbf{q}^i$  contains two contributions

$$\mathbf{q}^i = -D_s \nabla_i \mathbf{S} + V_i \mathbf{S}, \quad (3)$$

where the first term describes the spin-diffusion with coefficient  $D_s$  and the second term stems from the drag of the spin density with the drift velocity  $\mathbf{V} = \mathbf{e}_x V_x(y)$  determined by Eq. (1). For further consideration we also use the spin diffusion length  $L_s = \sqrt{D_s \tau_s}$  and the spin drift length  $L_d = V_* \tau_s$  in the centre of channel,  $V_* = V_x(W/2)$ .

In general, the spin diffusion length in high mobility samples can be extremely large due to long momentum relaxation times  $\tau_{tr}$ . For instance, in clean graphene-based lateral spin valves the spin can diffuse to a distance of up to 1  $\mu$ m [50–52]. However, when the viscous electron fluid is formed,  $D_s$  is significantly reduced [53] as it is mostly govern by electron-electron scattering, herewith

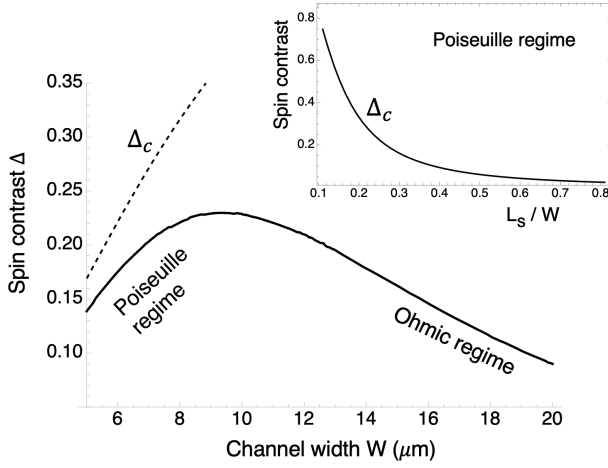


FIG. 3. The dependence of spin polarization contrast across the channel on its width  $W$ . The approximation  $\Delta_c$  from Eq. (4) is shown by the dotted curve. The inset shows the dependence  $\Delta_c$  on  $L_s/W$  for the Poiseuille regime.

the spin relaxation time  $\tau_s$  is controlled by D'yakonov-Perel-like mechanism giving  $1/\tau_s \sim \Omega_{so}^2 \tau_{ee}$  [54, 55]. The decrease of  $L_s$  due to the inter-particle scattering is favorable for the spin imaging of the Poiseuille flow, as the weakening of the spin diffusion prevents distortion of an inhomogeneous spin pattern.

The distribution of spin density  $S_z$  emerging due to the Poiseuille flow of electrons in the hydrodynamical regime at  $\omega_c = 0$  is demonstrated in Fig. 2(a). The parameters are relevant for high-mobility GaAs quantum wells [53, 55] and are described in the caption to Fig. 2, the channel width  $W = 8 \mu\text{m}$ .

As boundary conditions we used the absence of spin current  $q_y^z = 0$  at  $y = 0, W$ , we also assumed that  $q_x^z$  is proportional to the electric current flowing through the contact at  $x = 0$  [49]. In our case we take  $q_x^z \propto V_x(y)$  being consistent with the hydrodynamic distribution of the electric current in the bulk of the channel. We recognize that the electric current distribution right in the vicinity of a contact can alter from the Poiseuille form. However, beyond some transition region (no longer than  $x \lesssim W$ ) the drift velocity will be settled according to Eq. (1) and  $S_z$  will keep strongly inhomogeneous shape due to an effective dragging by  $\mathbf{E}$  in the center of the channel.

This feature is clearly seen in Fig. 2(b), where we demonstrate the profiles of the spin density across the channel at different distances from the left boundary. The tail of the spin distribution presented in Fig. 2(b) can be approximated by the expression

$$S_z(x, y) = A e^{-x/L_*} \left[ 1 - \Delta_c \cos\left(\frac{2\pi y}{W}\right) \right], \quad (4)$$

where  $A$  is a constant being independent of  $x$  and  $y$ , the factor  $e^{-x/L_*}$  describes the spin density decay with an averaged drift length  $L_* = \langle V_x \tau_s \rangle = 2L_d/3$  and the pa-

rameter  $\Delta_c$  determines the contrast of the spin imaging. It follows from Eq. 4 that imaging of the Poiseuille flow by spin injection is possible provided that  $\Delta_c \sim 1$ .

To determine the critical region beyond which  $\Delta_c$  vanishes we get an approximated analytical solution for Eq. (2). We use the biharmonic approximation for  $y$ -dependence of  $S_z(x, y)$  and  $V_x(y)$  and take into account only the drift component of  $q_x^z$ . For the slowest decaying solution at the tail of the spin density we obtain  $\Delta_c = 6/[2\pi^4 \xi^2 + \sqrt{18 + 72\pi^2 \xi^2 + 4\pi^8 \xi^4}]$ , where  $\xi = L_s/W$ . The expression Eq. (4) with  $\Delta_c$  from above is justified in range  $1 \lesssim \xi \lesssim 0.05$ , where the right boundary is determined by the failure of biharmonic approximation due to a weakened spin diffusion. The spin distribution plotted in Fig. 2 have the parameters  $\xi = 0.14$ ,  $\Delta_c = 0.52$  and the expression from Eq. (4) fits well with the numerical solution starting from  $x/W \gtrsim 1.2$ .

The dependence of  $\Delta_c$  on the ratio  $L_s/W$  is shown on the inset of Fig. 3. It is seen that the spin contrast decreases significantly  $\Delta_c \lesssim 0.2$  already at  $\xi \gtrsim 0.3$ , instead of  $\xi \gtrsim 1$  as might be expected. Since  $\Delta_c$  is determined by single ratio  $L_s/W$ , the applicability of the spin imaging approach for sufficiently large in-plane electric fields (when  $L_d \gg L_s$ ) is govern by a simple criteria  $W \gtrsim 3L_s$ , suggesting that a more plausible situation is realized for sufficiently wide samples. The spin contrast across the transition between Poiseuille and Ohmic transport regimes is illustrated in Fig. 3, where we present the dependence of  $\Delta = [S_z(y_c) - S_z(y_e)]/[S_z(y_c) + S_z(y_e)]$  on  $W$ ; here  $y_c = W/2$  is in the center of the channel and  $y_e = W/10$  is nearby its boundary. A nonmonotonic character of  $\Delta$  stems from the fast initial increase of  $\Delta_c(L_s/W)$  relevant for the Poiseuille flow, which is further suppressed at larger  $W$  due to the transition to the Ohmic regime.

Another spin-related evidence of the Poiseuille flow of the electron fluid revealed by the spin imaging technique is the appearance of nonzero relative phase shifts for the Hanle curves (the dependence of  $S_{z,x}$  on  $\omega_c \tau_s$ ) probed at different positions across the channel. Below we explain this idea in detail. We keep to the drift-dominated regime, at that the difference between two Larmor frequencies  $\Delta\omega_c$  at which the Hanle curve exhibits the neighboring peaks or dips at a fixed point of spin probe in space can be estimated as  $\Delta\omega_c = (2\pi V_x)/x_0$ , where  $x_0$  is the distance from the injector. In case of the Poiseuille electronic flow the drift velocity  $V_x(y)$  from Eq. (1) changes significantly across the channel leading to the variation of  $\Delta\omega_c$ . An ultimate manifestation of this feature would be the shift  $\Delta\omega_c$  as a function of  $y$ -coordinate at fixed distance  $x_0$  resulting in the “desynchronization” of the Hanle curves.

We proceed with considering this scenario in more detail. We apply an in-plane magnetic field  $\omega_c = \omega_c e_y$  and keep only the injection of  $S_z$  (the boundary conditions are the same as Fig. 2; the spin current  $q_x^x = 0$  is absent). In Fig. 4(a,b) we demonstrate inhomogeneous oscillating spatial patterns of  $S_z, S_x$  inside the electronic channel at

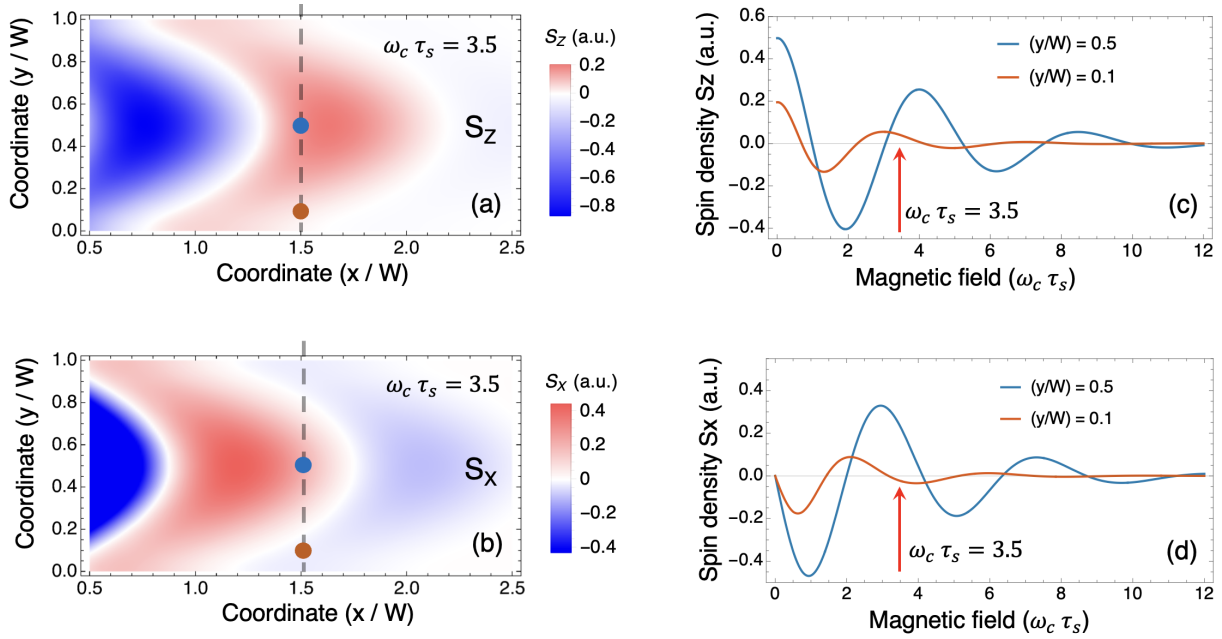


FIG. 4. Distribution of the spin density in magnetic field directed along the  $y$  axis. (a,b): Space-resolved densities  $S_z$  and  $S_x$  at  $\omega_c \tau_s = 3.5$ . (c,d): Magnetic field dependences of  $S_z$  and  $S_x$  calculated at  $x = 12 \mu\text{m}$  away from the injector. The Hanle curves on the right panels are taken at the center ( $y = 0.5W$ , blue color) and near the edge ( $y = 0.1W$ , orange color) of the channel. The positions of spin detection in each case are depicted by big dots of corresponded colors on the left panels.

fixed magnetic field  $\omega_c \tau_s = 3.5$  (red and blue colors stand for the positive and negative signs, respectively), other parameters are the same as in Fig. 2. The procession structure of the spin density visible in Fig. 4 is specific for the drift-dominated regime of the spin transport [49]. Importantly,  $S_{z,x}$  are sign-altering and inhomogeneous at the same moment, one can clearly observe that at fixed distance  $x_0$  the spin density can have different signs in the center and nearby the boundary of the channel. This feature is explicitly connected with the discussed variation in drift velocities emerging for the hydrodynamic regime of viscous electron fluid transport.

The relative shifts of the oscillations period  $\Delta\omega_c$  of the Hanle curves are shown in Fig. 4(c,d). The Hanle curves are calculated at two spatial positions across the channel, see Fig. 4(a,b). When  $\omega_c \tau_s \sim 4$ , these shifts are up to  $\pi$ . We argue that the presented desynchronization of the

Hanle curves upon hydrodynamical response can be used to confirm independently the formation of the viscous electron fluid.

In conclusion, we have proposed an approach to visualize hydrodynamic electronic flows by measuring the spin polarization distribution across the transport channel. Our calculations show that measuring both the spin polarization contrast and Hanle curves at the center and at the boundary of the channel allow one to disclose the hydrodynamic regime. We believe that the proposed method paves the way towards non-invasive studies of hydrodynamic viscous electron fluids in samples of different geometry and microscopic structure.

*Acknowledgements.* This work has been supported by the Russian Science Foundation (Project 18-72-10111). P.S.A. thanks the Theoretical Physics and Mathematics Advancement Foundation "BASIS".

- 
- [1] R. N. Gurzhi, *Sov. Phys. Uspekhi* **11**, 255 (1968).
  - [2] D. A. Bandurin, I. Torre, R. K. Kumar, M. Ben Shalom, A. Tomadin, A. Principi, G. H. Auton, E. Khestanova, K. S. Novoselov, I. V. Grigorieva, L. A. Ponomarenko, A. K. Geim, and M. Polini, *Science* **351**, 1055 (2016).
  - [3] R. Krishna Kumar, D. A. Bandurin, F. M. D. Pellegrino, Y. Cao, A. Principi, H. Guo, G. H. Auton, M. Ben Shalom, L. A. Ponomarenko, G. Falkovich, K. Watanabe, T. Taniguchi, I. V. Grigorieva, L. S. Levitov, M. Polini, and A. K. Geim, *Nature Physics* **13**, 1182 (2017).
  - [4] A. I. Berdyugin, S. G. Xu, F. M. D. Pellegrino, R. Krishna Kumar, A. Principi, I. Torre, M. Ben Shalom, T. Taniguchi, K. Watanabe, I. V. Grigorieva, M. Polini, A. K. Geim, and D. A. Bandurin, *Science* **364**, 162 (2019).
  - [5] S. Samaddar, J. Strasdas, K. Janßen, S. Just, T. Johnsen, Z. Wang, B. Uzlu, S. Li, D. Neumaier, M. Liebmann, *et al.*, *Nano Letters* **21**, 9365 (2021).
  - [6] L. Levitov and G. Falkovich, *Nature Physics* **12**, 672 (2016).
  - [7] J. A. Sulpizio, L. Ella, A. Rozen, J. Birkbeck, D. J.



- Perello, D. Dutta, M. Ben-Shalom, T. Taniguchi, K. Watanabe, T. Holder, R. Queiroz, A. Principi, A. Stern, T. Scaffidi, A. K. Geim, and S. Ilani, *Nature* **576**, 75 (2019).
- [8] M. J. H. Ku, T. X. Zhou, Q. Li, Y. J. Shin, J. K. Shi, C. Burch, L. E. Anderson, A. T. Pierce, Y. Xie, A. Hamo, U. Vool, H. Zhang, F. Casola, T. Taniguchi, K. Watanabe, M. M. Fogler, P. Kim, A. Yacoby, and R. L. Walsworth, *Nature* **583**, 537 (2019).
- [9] P. J. W. Moll, P. Kushwaha, N. Nandi, B. Schmidt, and A. P. Mackenzie, *Science* **351**, 1061 (2016).
- [10] J. Gooth, F. Menges, N. Kumar, V. Süß, C. Shekhar, Y. Sun, U. Drechsler, R. Zierold, C. Felser, and B. Gotsmann, *Nature Communications* **9**, 4093 (2018).
- [11] A. T. Hatke, M. A. Zudov, J. L. Reno, L. N. Pfeiffer, and K. W. West, *Phys. Rev. B* **85**, 081304 (2012).
- [12] R. G. Mani, A. Kriisa, and W. Wegscheider, *Scientific Reports* **3**, 2747 (2013).
- [13] L. Bockhorn, P. Barthold, D. Schuh, W. Wegscheider, and R. J. Haug, *Phys. Rev. B* **83**, 113301 (2011).
- [14] Q. Shi, P. D. Martin, Q. A. Ebner, M. A. Zudov, L. N. Pfeiffer, and K. W. West, *Phys. Rev. B* **89**, 201301 (2014).
- [15] P. S. Alekseev, *Phys. Rev. Lett.* **117**, 166601 (2016).
- [16] G. M. Gusev, A. D. Levin, E. V. Levinson, and A. K. Bakarov, *AIP Advances* **8**, 025318 (2018).
- [17] A. D. Levin, G. M. Gusev, E. V. Levinson, Z. D. Kvon, and A. K. Bakarov, *Phys. Rev. B* **97**, 245308 (2018).
- [18] G. M. Gusev, A. D. Levin, E. V. Levinson, and A. K. Bakarov, *Phys. Rev. B* **98**, 161303 (2018).
- [19] A. C. Keser, D. Q. Wang, O. Klochan, D. Y. H. Ho, O. A. Tkachenko, V. A. Tkachenko, D. Culcer, S. Adam, I. Farrer, D. A. Ritchie, O. P. Sushkov, and A. R. Hamilton, *Phys. Rev. X* **11**, 031030 (2021).
- [20] A. Gupta, J. J. Heremans, G. Kataria, M. Chandra, S. Fallahi, G. C. Gardner, and M. J. Manfra, *Phys. Rev. Lett.* **126**, 076803 (2021).
- [21] Y. L. Dai, R. R. Du, L. N. Pfeiffer, and K. W. West, *Phys. Rev. Lett.* **105**, 246802 (2010).
- [22] A. T. Hatke, M. A. Zudov, L. N. Pfeiffer, and K. W. West, *Phys. Rev. B* **83**, 121301 (2011).
- [23] M. Bialek, J. Lusakowski, M. Czapkiewicz, J. Wrobel, and V. Umansky, *Phys. Rev. B* **91**, 045437 (2015).
- [24] T. Scaffidi, N. Nandi, B. Schmidt, A. P. Mackenzie, and J. E. Moore, *Phys. Rev. Lett.* **118**, 226601 (2017).
- [25] H. Guo, E. Ilseven, G. Falkovich, and L. S. Levitov, *PNAS* **114**, 3068 (2017).
- [26] A. Lucas, *Phys. Rev. B* **95**, 115425 (2017).
- [27] F. M. D. Pellegrino, I. Torre, and M. Polini, *Phys. Rev. B* **96**, 195401 (2017).
- [28] P. S. Alekseev, I. V. Gornyi, A. P. Dmitriev, V. Y. Kachorovskii, and M. A. Semina, *Semiconductors* **51**, 766 (2017).
- [29] A. Lucas and K. C. Fong, *Journal of Physics: Condensed Matter* **30**, 053001 (2018).
- [30] O. Kashuba, B. Trauzettel, and L. W. Molenkamp, *Phys. Rev. B* **97**, 205129 (2018).
- [31] R. Moessner, P. Surówka, and P. Witkowski, *Phys. Rev. B* **97**, 161112 (2018).
- [32] M. Semenyakin and G. Falkovich, *Phys. Rev. B* **97**, 085127 (2018).
- [33] A. Lucas and S. Das Sarma, *Phys. Rev. B* **97**, 115449 (2018).
- [34] R. Cohen and M. Goldstein, *Phys. Rev. B* **98**, 235103 (2018).
- [35] P. S. Alekseev, *Phys. Rev. B* **98**, 165440 (2018).
- [36] J. Y. Khoo and I. S. Villadiego, *Phys. Rev. B* **99**, 075434 (2019).
- [37] P. S. Alekseev, *Semiconductors* **53**, 1367 (2019).
- [38] P. S. Alekseev and A. P. Alekseeva, *Phys. Rev. Lett.* **123**, 236801 (2019).
- [39] K. Trachenko and V. V. Brazhkin, *Sci. Adv.* **6**, eaba3747 (2020).
- [40] P. S. Alekseev and M. A. Semina, *Phys. Rev. B* **100**, 125419 (2019).
- [41] M. I. Dyakonov, *Phys. Rev. Lett.* **99**, 126601 (2007).
- [42] P. S. Alekseev and M. I. Dyakonov, *Phys. Rev. B* **100**, 081301 (2019).
- [43] M. Matsuo, Y. Ohnuma, and S. Maekawa, *Phys. Rev. B* **96**, 020401 (2017).
- [44] M. Matsuo, D. A. Bandurin, Y. Ohnuma, Y. Tsutsumi, and S. Maekawa, (2020), [arXiv:2005.01493 \[cond-mat.mes-hall\]](https://arxiv.org/abs/2005.01493).
- [45] R. Takahashi, M. Matsuo, M. Ono, K. Harii, H. Chudo, S. Okayasu, J. Ieda, S. Takahashi, S. Maekawa, and E. Saitoh, *Nature Physics* **12**, 52 (2016).
- [46] R. Takahashi, H. Chudo, M. Matsuo, K. Harii, Y. Ohnuma, S. Maekawa, and E. Saitoh, *Nature Communications* **11**, 3009 (2020).
- [47] R. J. Doornenbal, M. Polini, and R. A. Duine, *Journal of Physics: Materials* **2**, 015006 (2019).
- [48] M. M. Glazov, *2D Materials* **9**, 015027 (2021).
- [49] J. Fabian, A. Matos-Abiad, C. Ertler, P. Stano, and I. Žutić, *Semiconductor spintronics*, *Acta Physica Slovaca. Reviews and Tutorials* **57**, 565 (2007).
- [50] M. Drogeler, F. Volmer, M. Wolter, B. Terrés, K. Watanabe, T. Taniguchi, G. Guntherodt, C. Stampfer, and B. Beschoten, *Nano letters* **14**, 6050 (2014).
- [51] M. H. Guimarães, A. Veligura, P. Zomer, T. Maassen, I. Vera-Marun, N. Tombros, and B. Van Wees, *Nano Letters* **12**, 3512 (2012).
- [52] E. C. Ahn, 2d materials for spintronic devices, *npj 2D Materials and Applications* **4**, 1 (2020).
- [53] S. Anghel, F. Passmann, A. Singh, C. Ruppert, A. V. Poshakinskiy, S. A. Tarasenko, J. N. Moore, G. Yusa, T. Mano, T. Noda, X. Li, A. D. Bristow, and M. Betz, *Phys. Rev. B* **97**, 125410 (2018).
- [54] M. M. Glazov and E. L. Ivchenko, *JETP* **99**, 1279 (2004).
- [55] W. Leyland, G. John, R. Harley, M. Glazov, E. Ivchenko, D. Ritchie, I. Farrer, A. Shields, and M. Henini, *Physical Review B* **75**, 165309 (2007).